Computers and Mathematics with Applications 151 (2023) 288–299

Contents lists available at ScienceDirect

Computers and Mathematics with Applications

journal homepage: www.elsevier.com/locate/camwa

A semi-adaptive preservative scheme for a fractional quenching convective-diffusion problem

Nabing Liu [a], Lin Zhu [a,*], Qin Sheng [b]

[a] School of Mathematics and Statistics, Ningxia University, Yinchuan 750021, China
[b] Department of Mathematics and Center for Astrophysics, Space Physics and Engineering Research, Baylor University, Waco, TX 76798-7328, USA

ARTICLE INFO

Keywords:
Quenching problems
Singularity
Riemann-Liouville fractional derivatives
Preservative schemes
Numerical stability

ABSTRACT

A preservative scheme is presented and analyzed for the solution of a quenching type convective-diffusion problem modeled through one-sided Riemann-Liouville space-fractional derivatives. Properly weighted Grünwald formulas are employed for the discretization of the fractional derivative. A forward difference approximation is considered in the approximation of the convective term of the nonlinear equation. Temporal steps are optimized via an asymptotic arc-length monitoring mechanism till the quenching point. Under suitable constraints on spatial-temporal discretization steps, the monotonicity, positivity preservations of the numerical solution and numerical stability of the scheme are proved. Three numerical experiments are designed to demonstrate and simulate key characteristics of the semi-adaptive scheme constructed, including critical length, quenching time and quenching location of the fractional quenching phenomena formulated through the one-sided space-fractional convective-diffusion initial-boundary value problem. Effects of the convective function to quenching are discussed. Numerical estimates of the order of convergence are obtained. Computational results obtained are carefully compared with those acquired from conventional integer order quenching convection-diffusion problems for validating anticipated accuracy. The experiments have demonstrated expected accuracy and feasibility of the new method.

1. Introduction

Let $\Omega_a = (0, a),\ a > 0$. Consider the following one-dimensional (1D) γ-th order nonlinear convective-diffusion problem:

$$\frac{\partial h(x,t)}{\partial t} = d(x,t)\frac{\partial^\gamma h(x,t)}{\partial x^\gamma} + c(x,t)\frac{\partial h(x,t)}{\partial x} + p(h), x \in \Omega_a,\ t \in (0,T), \quad (1.1)$$

$$h(x,0) = \psi(x), \quad x \in \Omega_a, \quad (1.2)$$

$$h(0,t) = h(a,t) = 0, \quad t \in [0,T), \quad (1.3)$$

where $d(x,t) > 0$ and $1 < \gamma \le 2$. The nonnegative source function $p(h)$ is singular as h reaches certain thresholds. The fractional nonlinear model (1.1)-(1.3) delivers an accurate mathematical tool for describing many profound physical applications arising from nature and experimental sciences.

The above-mentioned one-sided convective-diffusion equation (OCDE) can be further viewed as a basic equation of motion. It models fluid flow and heat transfer, combustion and explosion, or cooling reactions in the industry [1]. The quenching phenomena it intends to interpret can also be found in biochemical reactions in drug productions, electrochemical cells [2], and temperature-dependent thermal coefficients [3] and so on. Therefore, the research of reliable numerical solutions of (1.1)-(1.3) carries high theoretical and practical values.

There have been multiple ways for solving quenching type singular equations. For example, a local projection stabilization virtual element method was applied for solving a similar convection-diffusion-reaction problem [4]. Super convergence of finite element method with singularly perturbed system was observed in 1D modeling equation simulations [5]. For the algorithmic simplicity and practical effectiveness, the most commonly used numerical procedures in the territory remain to be finite difference based [6–8].

Consider the nonlinear source function

$$p(h) = (L-h)^{-\theta}, \quad 0 \le h < L, \quad (1.4)$$

where $\theta > 0$ is the physical combustion index [3,9]. Apparently, $p(h)$ is strictly increasing for $0 \le h < L$ with $p(0) = 1/L^\theta > 0$, and $p(h) \to +\infty$, as $h \to L^-$.

* Corresponding author.
E-mail addresses: liunb_nxu@163.com (N. Liu), zhul@nxu.edu.cn (L. Zhu), qin_sheng@baylor.edu (Q. Sheng).

https://doi.org/10.1016/j.camwa.2023.09.043
Received 9 March 2023; Received in revised form 19 August 2023; Accepted 22 September 2023

In 1975, Kawarada first mentioned the quenching phenomenon due to (1.4) with $\theta = 1$. A necessary condition for a quenching was also given in [10]. It was proved that for Kawarada's original modeling equation, $h_t = h_{xx} + 1/(1-h)$, $x \in (0,a)$, $t > 0$, there must exist a critical size $a^\star \in (2\sqrt{2}, +\infty)$ such that $\forall\, a > a^\star$, there exists a unique $T_a < \infty$, and $\sup\limits_{x\in(0,a)} \lim\limits_{t\to T_a^-} h = 1$ [10,11]. Walter and Acker later verified this result and discovered that $a^\star \approx 1.5303$ by means of simulation experiments [12]. The monotonicity, stability and positivity of a quenching solution are proposed and investigated in numerous publications either analytically or numerically later on, including substantial work implemented by Zhu, Sheng et al. for fractional order quenching type convective-diffusion equations [13,14]. The simulation methods constructed are far more balanced and effective as compared to traditional unilateral and composite finite difference approaches [15].

In our present study, we are particularly interested in semi-adaptive computations of the numerical solution of quenching type fractional order quenching problems. Although such solutions of fractional order quenching models can be found in numerous recent publications (see [7,13,14,16] and references therein), the numerical approach for OCDE problems such as (1.1)-(1.3) equipped with the one-sided Riemann-Liouville (R-L) space-fractional diffusion term and convective term remain unsolved. This motivates the present study. Our paper successfully extends the work of [13], and accomplishes investigations of preservative features such as the positivity, monotonicity and stability for numerical solutions acquired and quenching characteristics validations for $\dfrac{\sqrt{17}-1}{2} \le \gamma \le 2$ [13,17].

The remaining structure of this study consists of the following five interactive parts. A semi-discretized fractional order quenching model approximation and a semi-adaptive scheme will be introduced and discussed in Section 2. In Section 3, the numerical stability of the semi-adaptive scheme will be investigated and analyzed. Preservation features and characteristics will be studied in Section 4. Emphases will be given to verifications of the solution positivity and monotonicity. Section 5 is devoted to numerical experiments and simulations of quenching phenomena associated with the modeling problem (1.1)-(1.3). Three sets of experiments will be given on critical lengths, quenching times and quenching location respectively. Numerical solutions will be compared with existing results and simulations. Estimates of the order of convergence are calculated. Finally, straightforward conclusions and continuing endeavors will be presented in Section 6.

2. Semi-adaptive difference scheme

For problem (1.1)-(1.3), we stipulate the space-time interval $[0,a]\times[0,T]$ by a $N\times K$ grid, where $N, K \in \mathbb{Z}^+$ and are far greater than 1. Let $\lambda = a/N$, $\tau = T/K$. We define following mesh region,

$$\bar{\Omega}_{a,\lambda} \times T_\tau = \left\{(x_i, t_k) :\ x_i = i\lambda,\ t_k = k\tau,\ \ i = 0,1,2,\dots,N;\ k = 0,1,\dots,K\right\}.$$

Furthermore, we denote $d_i = d(x_i,t), c_i = c(x_i,t)$ and $h_i = h(x_i,t)$, $i = 0,1,2,\dots,N$. Let $p_i = p(h_i)$. Then standard and shifted Grünwald formulas [6] for (1.1) are defined respectively as

$$\begin{aligned}
\frac{\partial^\gamma h(x,t)}{\partial x^\gamma} &= \lim_{\lambda\to 0^+} \frac{1}{\lambda^\gamma} \sum_{m=0}^{N} z_m h(x - m\lambda, t) + \mathcal{O}(\lambda);\\
\frac{\partial^\gamma h(x,t)}{\partial x^\gamma} &= \lim_{\lambda\to 0^+} \frac{1}{\lambda^\gamma} \sum_{m=0}^{N} z_m h(x - (m-1)\lambda, t) + \mathcal{O}(\lambda),
\end{aligned} \tag{2.1}$$

where

$$z_m = \frac{\Gamma(m-\gamma)}{\Gamma(-\gamma)\Gamma(m+1)} = (-1)^m \frac{\gamma(\gamma-1)\cdots(\gamma-m+1)}{m!}, \quad m = 0,1,\dots,N.$$

It is readily to see from the z_m formulas that

$$\begin{aligned}
&(a)\ z_0 = 1;\ \ (b)\ -z_1 = \gamma > 0;\ \ (c)\ 0 \le z_{m+1} \le z_m \le 1,\ \text{if } m \ge 2;\\
&(d)\ \textstyle\sum_{m=0}^{N} z_m \le 0,\ N \in \mathbb{Z}^+;\ \ (e)\ \sum_{m=0}^{\infty} z_m = 0.
\end{aligned} \tag{2.2}$$

It is shown in [17] that

$$\frac{\partial^\gamma h(x_k,t)}{\partial x^\gamma} = \frac{1}{\lambda^\gamma}\left[\left(1-\frac{\gamma}{2}\right)\sum_{j=0}^{k} z_j h_{k-j} + \frac{\gamma}{2}\sum_{j=0}^{k+1} z_j h_{k-j+1}\right] + \mathcal{O}(\lambda^2), \quad \lambda \to 0^+. \tag{2.3}$$

We discretize the convective term of (1.1) via the standard forward differential formula, that is,

$$\frac{\partial h(x_k,t)}{\partial x} = \frac{h_{k+1} - h_k}{\lambda} + \mathcal{O}(\lambda), \quad \lambda \to 0^+. \tag{2.4}$$

An application of (2.3) and (2.4) to (1.1) yields the following semi-discretized differential system,

$$\begin{aligned}
(h')_k = \frac{d_k}{\lambda^\gamma}&\left[\left(1-\frac{\gamma}{2}\right)\sum_{j=0}^{k} z_j h_{k-j} + \frac{\gamma}{2}\sum_{j=0}^{k+1} z_j h_{k-j+1}\right] + \frac{c_k}{\lambda}(h_{k+1} - h_k) + p_k,\\
&k = 1,2,\dots,N.
\end{aligned}$$

The above system can be compressed into a vector form:

$$h' = Vh + p(h), \quad 0 < t < T; \quad h(0) = h_0, \tag{2.5}$$

where $h = (h_1, h_2, \dots, h_N)^\intercal \in \mathbb{R}^N$, $p = (p_1, p_2, \dots, p_N)^\intercal \in \mathbb{R}^N$ and $V = (v_{ij}) \in \mathbb{R}^{N\times N}$ for which

$$v_{ij} = \begin{cases}
\dfrac{d_i}{\lambda^\gamma}\left[\left(1-\frac{\gamma}{2}\right)z_0 + \frac{\gamma}{2}z_1\right] - \dfrac{c_i}{\lambda}, & i = j;\\
\dfrac{d_i}{\lambda^\gamma}\left[\left(1-\frac{\gamma}{2}\right)z_{i-j} + \frac{\gamma}{2}z_{i-j+1}\right], & i > j;\\
\dfrac{d_i\gamma z_0}{2\lambda^\gamma} + \dfrac{c_i}{\lambda}, & i = j-1;\\
0, & \text{otherwise.}
\end{cases}$$

A formal solution of the initial value problem (2.5) can be expressed as

$$h(t+\tau) = e^{\tau V} h(t) + \int_t^{t+\tau} e^{(t+\tau-\xi)V} p(h(\xi))\, d\xi, \quad t, \tau \ge 0.$$

In the circumstance when $\tau \to 0^+$, applying the trapezoidal rule for the integral, we acquire the following fully discretized approximation from the above exact solution:

$$h(t+\tau) = \frac{\tau}{2}p(h(t+\tau)) + \frac{\tau}{2}e^{\tau V}p(h(t)) + e^{\tau V}h(t) + \mathcal{O}(\tau^2), \quad t \in [0,T). \tag{2.6}$$

Consider an A-stable [1/1] Padé formula for the matrix exponential $e^{\tau V}$, that is,

$$e^{\tau V} = \left(I - \frac{\tau}{2}V\right)^{-1}\left(I + \frac{\tau}{2}V\right) + \mathcal{O}(\tau^2), \quad \tau \to 0^+. \tag{2.7}$$

Combine (2.6) with (2.7) and drop the truncation error terms. We obtain immediately the following second-order fully discretized semi-adaptive scheme:

$$h_n = \left(I - \frac{\tau_n}{2}V\right)^{-1}\left(I + \frac{\tau_n}{2}V\right)\left(h_{n-1} + \frac{\tau_n}{2}p_{n-1}\right) + \frac{\tau_n}{2}p_n, \ n = 1,2,\dots,K \tag{2.8}$$

$$h_0 = (h_1(0), h_2(0), \dots, h_K(0))^\intercal, \tag{2.9}$$

where $0 < \tau_n = t_n - t_{n-1} \ll 1$, $n = 1,2,\dots,K$, can be determined via a proper adaptation mechanism. The algorithm (2.8) is highly nonlinear and implicit. In realistic simulations, a straightforward explicit approximation, such as the forward Euler method, can be employed to linearize the procedure: $p_n \approx p(h_{n-1} + \tau_n(Vh_{n-1} + p_{n-1}))$ [8,9,18]. But the Euler formula reduces the order in temporal direction to linear. Therefore the best overall truncation error is of $\mathcal{O}(\lambda + \tau_n)$ for (2.8) (2.9). This actually coincides the Courant number requirement [19]. It has been demonstrated by many authors that a linearization can be extremely valuable even when strong quenching singularities are present [9,15,20]. In our study, we are particularly interested in following arc-length monitor function of the derivative function h' [9,15].

$$l(h',t) = \sqrt{1 + (h'')^2}, \quad t \in [0, +\infty).$$

Given values τ_0 and τ_1. We use the following quadratic formula for variable time steps when $n = 2, 3, \ldots, K$,

$$\tau_{i,n}^2 = \tau_{i,n-1}^2 + [(h')_{i,n-1} - (h')_{i,n-2}]^2 - [(h')_{i,n} - (h')_{i,n-1}]^2, \quad i = 0, 1, \ldots, N. \tag{2.10}$$

Set $\tau_n = \frac{1}{N}\sum_{i=0}^{N} \tau_{i,n}$. Under the appropriate smoothness constraints [8, 21], we may proceed ahead for calculating required adaptive time steps through the recursive relations (2.10).

3. Numerical stability

Theorem 3.1. *If* $\left(\sqrt{17}-1\right)/2 \le \gamma \le 2$ *then the matrix* $I - (\tau_n/2)V$ *is inverse positive, strictly diagonally dominant and monotone.*

Proof. Set $A = I - (\tau_n/2)V = (a_{ij}) \in \mathbb{R}^{N\times N}$. It follows that

$$\begin{aligned}
a_{kk} &= 1 - \frac{\tau_n d_k}{2\lambda^\gamma}\left[\left(1-\frac{\gamma}{2}\right)z_0 + \frac{\gamma}{2}z_1\right] + \frac{\tau_n c_k}{2\lambda} \\
&= 1 + \frac{\tau_n d_k}{2\lambda^\gamma}\left(\frac{\gamma^2}{2} + \frac{\gamma}{2} - 1\right) + \frac{\tau_n c_k}{2\lambda}, \quad k = 1, 2, \ldots, N, \\
a_{k,k+1} &= -\frac{\tau_n}{2}\left[\frac{d_k\gamma}{2\lambda^\gamma}z_0 + \frac{c_k}{\lambda}\right], \quad k = 1, 2, \ldots, N-1, \\
a_{k,j} &= -\frac{\tau_n d_k}{2\lambda^\gamma}\left[\left(1-\frac{\gamma}{2}\right)z_{k-j} + \frac{\gamma}{2}z_{k-j+1}\right], \ j < k, \quad k = 2, 3, \ldots, N.
\end{aligned}$$

We consider the following constraints:

$$\frac{\sqrt{17}-1}{2} \le \gamma \le 2. \tag{3.1}$$

It may readily be seen that [17]

$$\begin{aligned}
&\tfrac{\gamma}{2}z_{k-j+1} + \left(1-\tfrac{\gamma}{2}\right)z_{k-j} > 0, \quad j < k, \ k = 2, 3, \ldots, N, \\
&\tfrac{\gamma^2}{2} + \tfrac{\gamma}{2} - 1 > 0.
\end{aligned} \tag{3.2}$$

By definitions we also have properties

$$\begin{aligned}
&a_{kk} > 0, \ k = 1, 2, \ldots, N; \quad a_{k,k+1} < 0, \ k = 1, 2, \ldots, N-1; \\
&a_{k,j} < 0, \ j < k, \ k = 2, 3, \ldots, N.
\end{aligned}$$

On the other hand, summing up absolute values of off-diagonal elements of A yields the following,

$$\begin{aligned}
r_i &= \sum_{j=1, j\neq i}^{N}\left|a_{ij}\right| = \frac{\tau_n c_i}{2\lambda} + \frac{\tau_n d_i \gamma}{4\lambda^\gamma}z_0 + \frac{\tau_n d_i}{2\lambda^\gamma}\left\{\sum_{l=1}^{i-1}\left[\frac{\gamma}{2}z_{i-l+1} + \left(1-\frac{\gamma}{2}\right)z_{i-l}\right]\right\} \\
&= \frac{\tau_n c_i}{2\lambda} + \frac{\tau_n d_i}{2\lambda^\gamma}\left[\frac{\gamma}{2}\sum_{j=0, j\neq 1}^{i} z_j + \left(1-\frac{\gamma}{2}\right)\sum_{j=1}^{i-1} z_j\right] \\
&\le \frac{\tau_n c_i}{2\lambda} + \frac{\tau_n d_i}{2\lambda^\gamma}\left[\frac{\gamma}{2}\times(-z_1) + \left(1-\frac{\gamma}{2}\right)\times(-z_0)\right] \\
&= \frac{\tau_n c_i}{2\lambda} + \frac{\tau_n d_i}{2\lambda^\gamma}\left(\frac{\gamma^2}{2} + \frac{\gamma}{2} - 1\right), \quad i = 2, 3, \ldots, N.
\end{aligned}$$

Therefore,

$$r_i = \sum_{j=1, j\neq i}^{N}\left|a_{ij}\right| < \frac{\tau_n c_i}{2\lambda} + \frac{\tau_n d_i}{2\lambda^\gamma}\left(\frac{\gamma^2}{2} + \frac{\gamma}{2} - 1\right) + 1 = a_{ii}, \quad i = 2, 3, \ldots, N.$$

A particular case is for $i = 1$, we have $|a_{12}| \le a_{11}$ due to (3.1). These imply that A is strictly diagonally dominant and it is therefore invertible.

Now, according to (2.2), we observe that

$$\sum_{j=0}^{i-1} z_j \le 0, \ i = 2, 3, \ldots, N; \quad \sum_{j=0}^{i} z_j \le 0, \quad \sum_{j=1}^{i} z_j \le -1, \quad i = 1, 2, \ldots, N.$$

Hence,

$$\sum_{j=1}^{N} a_{ij} = 1 - \frac{\tau_n d_i}{2\lambda^\gamma}\left[\left(1-\frac{\gamma}{2}\right)\sum_{j=0}^{i-1} z_j + \frac{\gamma}{2}\sum_{j=0}^{i} z_j\right] > 0, \quad i = 1, 2, \ldots, N-1.$$

In the case if $i = N$, then we have

$$\sum_{j=1}^{N} a_{Nj} = 1 - \frac{\tau_n d_i}{2\lambda^\gamma}\left[\left(1-\frac{\gamma}{2}\right)\sum_{j=0}^{N-1} z_j + \frac{\gamma}{2}\sum_{j=1}^{N} z_j\right] > 0.$$

Consequently, the matrix A meets all conditions of the weak-row sum criterions [22], therefore it is strictly monotone and inversely positive. This completes our proof. □

Theorem 3.2. *Denote* $d_{\max} = \max_{1\le k\le N} d_k$, $c_{\max} = \max_{1\le k\le N} c_k$, $\beta_{\gamma,n} = \max_n \frac{\tau_n}{\lambda^\gamma}$. *If*

$$\beta_{\gamma,n} \le \frac{1}{2\left(d_{\max} + c_{\max}\right)}, \quad \frac{\sqrt{17}-1}{2} \le \gamma \le 2 \tag{3.3}$$

then $I + \frac{\tau_n}{2}V$ *is positive and nonsingular.*

Proof. Set $B = I + \frac{\tau_n}{2}V = (b_{ij}) \in \mathbb{R}^{N\times N}$, where

$$\begin{aligned}
b_{ii} &= 1 + \frac{\tau_n d_i}{2\lambda^\gamma}\left[\left(1-\frac{\gamma}{2}\right)z_0 + \frac{\gamma}{2}z_1\right] - \frac{\tau_n c_i}{2\lambda} \\
&= 1 - \frac{\tau_n d_i}{2\lambda^\gamma}\left(\frac{\gamma^2}{2} + \frac{\gamma}{2} - 1\right) - \frac{\tau_n c_i}{2\lambda}, \quad i = 1, 2, \ldots, N, \\
b_{i,i+1} &= \frac{\tau_n}{2}\left[\frac{d_k\gamma}{2\lambda^\gamma}z_0 + \frac{c_i}{\lambda}\right], \quad i = 1, 2, \ldots, N-1, \\
b_{i,j} &= \frac{\tau_n d_i}{2\lambda^\gamma}\left[\left(1-\frac{\gamma}{2}\right)z_{i-j} + \frac{\gamma}{2}z_{i-j+1}\right], \quad j < i, \ i = 2, 3, \ldots, N.
\end{aligned}$$

Firstly, similar to the proof of last theorem, the positivity of diagonal elements of B can be readily shown through (3.2) and (3.3). Secondly, we may study the infinite norm of $\frac{\tau_n}{2}V$. To this end,

$$\begin{aligned}
\left\|\frac{\tau_n}{2}V\right\|_\infty &= \max_i\left\{\frac{\tau_n}{2}\sum_{j=1}^{N}\left|V_{ij}\right|\right\} \\
&= \max_i\left\{\frac{\tau_n d_i}{2\lambda^\gamma}\left[\sum_{j=1}^{i-1}\left(\frac{\gamma}{2}z_{i-j+1} + (1-\frac{\gamma}{2})z_{i-j}\right) + \frac{\gamma}{2}z_0 - \left(\frac{\gamma}{2}z_1 + (1-\frac{\gamma}{2})z_0\right)\right] + \frac{\tau_n c_i}{\lambda}\right\} \\
&= \frac{\tau_n d_i}{2\lambda^\gamma}\max_i\left\{\sum_{j=1}^{i-1}\left(\frac{\gamma}{2}z_{i-j+1} + (1-\frac{\gamma}{2})z_{i-j}\right) + \frac{\gamma}{2}z_0 - \left(\frac{\gamma}{2}z_1 + (1-\frac{\gamma}{2})z_0\right)\right\} + \max_i\frac{\tau_n c_i}{\lambda} \\
&\le \frac{\max_n(\tau_n)d_{\max}}{\lambda^\gamma}\left(\frac{\gamma^2}{2} + \frac{\gamma}{2} - 1\right) + \frac{\max_n(\tau_n)c_{\max}}{\lambda^\gamma}.
\end{aligned}$$

Furthermore, when $\beta_{\gamma,n} \le \frac{1}{2(d_{max} + c_{max})}$, we may see that $\left\|\frac{\tau_n}{2}V\right\|_\infty < 1$. Thus, B must be nonsingular according to [22]. □

Definition 3.1. [23] Let $\tilde{h}^n$, h^n denote the perturbed and true solutions of a numerical method, respectively. Set $E^n = h^n - \tilde{h}^n$, $0 \le n \le K$. We say that the numerical method is stable if there is a suitable Euclidean norm $\|\cdot\|$ such that $\|E^n\| \le c\left\|E^0\right\|$, $0 \le n \le K$ hold, where $c > 0$ is a constant. We say that the numerical method is conditionally stable if the inequalities hold only when some constraints are satisfied.

Theorem 3.3. *Suppose the source function* p *be frozen. If* (3.3) *holds, then the semi-adaptive method* (2.8),(2.9) *is conditionally stable.*

Proof. Suppose function $p(h)$ be frozen, that is, h be fixed. Denote $\xi_\chi^k = \tau_k d_\chi/(2\lambda^\gamma)$, $\omega_\chi^k = \tau_k c_\chi/(2\lambda)$, $\chi = 1, 2, \ldots, N$, $k = 0, 1, \ldots, K$. We may obtain the following identities:

$$\left(I - \frac{\tau_k}{2}V\right)E^{k+1} = \left(I + \frac{\tau_k}{2}V\right)E^k, \quad k = 0, 1, \ldots, K-1,$$

following (2.8) and Definition 3.1.

On account of the above remark, we use a mathematical induction to prove that $\|E^n\| \le \left\|E^0\right\|$, $0 \le n \le K$. First of all, when $n = 1$, on the basis of (3.2) we acquire that

$$\begin{aligned}
\left\|E^1\right\|_\infty &= \max_{1\le j\le N}\left|E_j^1\right| = \left|E_\chi^1\right| \le \left|E_\chi^1\right| - \xi_\chi^1\left(1-\frac{\gamma}{2}\right)\sum_{m=0}^{\chi-1} z_m\left|E_\chi^1\right| \\
&\quad - \xi_\chi^1\frac{\gamma}{2}\sum_{m=0}^{\chi} z_m\left|E_\chi^1\right| + \omega_\chi^1\left|E_\chi^1\right| - \omega_\chi^1\left|E_\chi^1\right| \\
&\le \left[1-\xi_\chi^1\left(1-\frac{\gamma}{2}\right)z_0 - \xi_\chi^1\frac{\gamma}{2}z_1 + \omega_\chi^1\right]\left|E_\chi^1\right| - \left[\xi_\chi^1\frac{\gamma}{2}z_0 + \omega_\chi^1\right]\left|E_{\chi+1}^1\right| \\
&\quad -\xi_\chi^1\sum_{m=2}^{\chi}\left[\left(1-\frac{\gamma}{2}\right)z_{m-1} + \frac{\gamma}{2}z_m\right]\left|E_{\chi-m+1}^1\right| \\
&= \left[1+\xi_\chi^0\left(1-\frac{\gamma}{2}\right)z_0 + \xi_\chi^0\frac{\gamma}{2}z_1 - \omega_\chi^0\right]\left|E_\chi^0\right| + \left[\xi_\chi^0\frac{\gamma}{2}z_0 + \omega_\chi^0\right]\left|E_{\chi+1}^0\right| \\
&\quad +\xi_\chi^0\sum_{m=2}^{\chi}\left[\left(1-\frac{\gamma}{2}\right)z_{m-1} + \frac{\gamma}{2}z_m\right]\left|E_{\chi-m+1}^0\right| \\
&\le \left[1+\left(1-\frac{\gamma}{2}\right)\xi_\chi^0\sum_{m=0}^{\chi-1} z_m + \frac{\gamma}{2}\xi_\chi^0\sum_{m=0}^{\chi} z_m\right]\max_{1\le j\le K}\left|E_j^0\right| \\
&\le \max_{1\le j\le K}\left|E_j^0\right| = \left\|E^0\right\|_\infty.
\end{aligned}$$

Particularly if $\left\|E^1\right\|_\infty = \left|E_N^1\right|$, we have in (2.1) that

$$\begin{aligned}
\left\|E^1\right\|_\infty &= \left|E_N^1\right| \le \left|E_N^1\right| - \xi_N^1\left(1-\frac{\gamma}{2}\right)\sum_{m=0}^{N-1} z_m\left|E_N^1\right| \\
&\quad - \xi_N^1\frac{\gamma}{2}\sum_{m=0}^{N} z_m\left|E_N^1\right| + \omega_N^1\left|E_N^1\right| \\
&\le \left[1-\xi_N^1\left(1-\frac{\gamma}{2}\right)z_0 - \xi_N^1\frac{\gamma}{2}z_1 + \omega_N^1\right]\left|E_N^1\right| \\
&\quad -\xi_N^1\sum_{m=2}^{N}\left[\left(1-\frac{\gamma}{2}\right)z_{m-1} + \frac{\gamma}{2}z_m\right]\left|E_{N-m+1}^1\right| \\
&= \left[1+\xi_N^0\left(1-\frac{\gamma}{2}\right)z_0 + \xi_N^0\frac{\gamma}{2}z_1 - \omega_N^0\right]\left|E_N^0\right| \\
&\quad +\xi_N^0\sum_{m=2}^{N}\left[\left(1-\frac{\gamma}{2}\right)z_{m-1} + \frac{\gamma}{2}z_m\right]\left|E_{N-m+1}^0\right| \\
&\le \left[1+\left(1-\frac{\gamma}{2}\right)\xi_N^0\sum_{m=0}^{N-1} z_m + \frac{\gamma}{2}\xi_N^0\sum_{m=0}^{N} z_m\right]\max_{1\le j\le K}\left|E_j^0\right| \\
&\le \max_{1\le j\le K}\left|E_j^0\right| = \left\|E^0\right\|_\infty. \qquad (3.4)
\end{aligned}$$

Furthermore, suppose that $\|E^n\|_\infty \le \left\|E^0\right\|_\infty$ for $n = 1, 2, \ldots, k-1$. Thus, due to (2.1) and (3.3), for $n = k$ $(k > 1)$ we arrive consequently at

$$\begin{aligned}
\|E^n\|_\infty &= \max_{1\le j\le N}\left|E_j^n\right| = \left|E_\chi^n\right| \le \left|E_\chi^n\right| - \xi_\chi^n\left(1-\frac{\gamma}{2}\right)\sum_{m=0}^{\chi-1} z_m\left|E_\chi^n\right| \\
&\quad - \xi_\chi^n\frac{\gamma}{2}\sum_{m=0}^{\chi} z_m\left|E_\chi^n\right| + \omega_\chi^n\left|E_\chi^n\right| - \omega_\chi^n\left|E_\chi^n\right| \\
&\le \left[1-\xi_\chi^n\left(1-\frac{\gamma}{2}\right)z_0 - \xi_\chi^n\frac{\gamma}{2}z_1 + \omega_\chi^n\right]\left|E_\chi^n\right| - \left[\xi_\chi^n\frac{\gamma}{2}z_0 + \omega_\chi^n\right]\left|E_{\chi+1}^n\right| \\
&\quad -\xi_\chi^n\sum_{m=2}^{\chi}\left[\left(1-\frac{\gamma}{2}\right)z_{m-1} + \frac{\gamma}{2}z_m\right]\left|E_{\chi-m+1}^n\right| \\
&\le \left[1+\left(1-\frac{\gamma}{2}\right)\xi_\chi^{n-1}\sum_{m=0}^{\chi-1} z_m + \frac{\gamma}{2}\xi_\chi^{n-1}\sum_{m=0}^{\chi} z_m\right]\max_{1\le j\le K}\left|E_j^{n-1}\right| \\
&\le \max_{1\le j\le K}\left|E_j^{n-1}\right| = \left\|E^{n-1}\right\|_\infty.
\end{aligned}$$

In particularly if $\|E^n\|_\infty = \left\|E_N^n\right\|$ then $\left\|E^k\right\|_\infty \le \left|E_N^0\right|$ is true. This is the same as in the proof of (3.4). Recalling our assumption, we deduce that $\|E^n\|_\infty \le \left\|E^0\right\|_\infty$ for all $n \in \{1, 2, \cdots, K\}$, which completes the proof. □

4. Preservation analysis

Nonlinear quenching problems of the type (1.1)-(1.3) have been known for their abundant features relevant to multiple physics applications, particularly in cell biological simulations and solid fuel combustion [8,12,24]. It is expected that the numerical solution sequence $\{h^n\}_{n=0}^K$ produced by (2.8), (2.9) must be positive and strictly monotonically increasing [9,15,21].

Lemma 4.1. *Suppose $h_0 = 0$ and $\tau_1 > 0$ being an initial time step. Further, assume that $\tau_1 < \sigma^{-1}$ and (3.3) hold, where $\sigma = \max(p(\tau_1 p_0))$. Then $h_1 > h_0$ and $\|h_1\|_\infty < 1$.*

Proof. From (2.8), we may observe that

$$\begin{aligned}
h_1 &= \left(I-\frac{\tau_1}{2}V\right)^{-1}\left(I+\frac{\tau_1}{2}V\right)\left(h_0+\frac{\tau_1}{2}p_0\right) + \frac{\tau_1}{2}p_1 \\
&= \frac{\tau_1}{2}\left[\left(I-\frac{\tau_1}{2}V\right)^{-1}\left(I+\frac{\tau_1}{2}V\right)p_0 + p(\tau_1 p_0)\right].
\end{aligned}$$

Therefore, $h_1 > h_0 = 0$ owing to Theorems 3.1 and 3.2. We further demonstrate that $\|h_1\|_\infty < 1$. Let X be a column vector and each of its components is one. We consider the difference

$$h_1 - X = \left(I-\tfrac{\tau_1}{2}V\right)^{-1}\left[\tfrac{\tau_1}{2}\left(I+\tfrac{\tau_1}{2}V\right)p_0 + \tfrac{\tau_1}{2}\left(I-\tfrac{\tau_1}{2}V\right)p(\tau_1 p_0) - \left(I-\tfrac{\tau_1}{2}V\right)X\right].$$

Set

$$G_1 = \frac{\tau_1}{2}\left(I+\frac{\tau_1}{2}V\right)p_0 + \frac{\tau_1}{2}\left(I-\frac{\tau_1}{2}V\right)p(\tau_1 p_0),\ G_2 = -\left(I-\frac{\tau_1}{2}V\right)X.$$

Recall (2.2). It is readily to see that $VX \le 0$. So, apparently that $G_2 \le -X$. Now,

$$G_1 \le \frac{\tau_1}{2}\left[\left(I-\frac{\tau_1}{2}V\right) + \left(I+\frac{\tau_1}{2}V\right)\right]p(\tau_1 p_0) = \tau_1 p(\tau_1 p_0).$$

Hence,

$$\begin{aligned}
h_1 - X &= \left(I-\frac{\tau_1}{2}V\right)^{-1}(G_1+G_2) \le \left(I-\frac{\tau_1}{2}V\right)^{-1}\left(\tau_1 p(\tau_1 p_0) - X\right) \\
&< \left(I-\frac{\tau_1}{2}V\right)^{-1}(\tau_1\max(p(\tau_1 p_0)) - 1) = \left(I-\frac{\tau_1}{2}V\right)^{-1}(\tau_1\sigma - 1).
\end{aligned}$$

Recall Theorem 3.1. For $\tau_1 < \sigma^{-1}$, we find immediately that $h_1 < X$. Furthermore, $\|h_1\|_\infty < 1$. Our proof is thus completed. □

Lemma 4.2. *Suppose (3.3) be true. Then for any considerably small time step $\tau_n > 0$ and $0 \le h_{n-1} < 1$, satisfying $Vh_{n-1} + p_{n-1} > 0$, the solution vectors generated by (2.8) are strictly monotonically increasing with $Vh_n + p_n > 0$ ensured.*

Proof. Recall Lemma 4.1. Property $h_1 > h_0$ is secured. Considering an Euler formula for p_n, that is,

$$p_n = p_{n-1} + \tau_n M(Vh_{n-1} + p_{n-1}) + \mathcal{O}(\tau_n^2), \quad n \ge 1, \qquad (4.1)$$

where M is the diagonal Jacobian matrix of $p(h)$ that is positive. Utilizing (2.8), we get

$$\begin{aligned}
h_n - h_{n-1} &= \left(I-\frac{\tau_n}{2}V\right)^{-1}\left[\left(I+\frac{\tau_n}{2}V\right)\left(h_{n-1}+\frac{\tau_n}{2}p_{n-1}\right)\right. \\
&\quad \left. + \frac{\tau_n}{2}\left(I-\frac{\tau_n}{2}V\right)p_n - \left(I-\frac{\tau_n}{2}H\right)h_{n-1}\right] \\
&= \left(I-\frac{\tau_n}{2}V\right)^{-1}\left[\tau_n Vh_{n-1} + \frac{\tau_n}{2}p_{n-1} + \frac{\tau_n}{2}p_n + \frac{\tau_n^2}{4}V(p_{n-1}-p_n)\right] \\
&\ge \tau_n\left(I-\frac{\tau_n}{2}V\right)^{-1}\left[Vh_{n-1} + p_{n-1} - \frac{\tau_n}{4}V(p_n - p_{n-1})\right], \quad n > 1.
\end{aligned}$$

Owing to (4.1), we observe that

$$h_n - h_{n-1} \geq \tau_n \left(I - \tfrac{\tau_n}{2}V\right)^{-1} \left[(Vh_{n-1} + p_{n-1}) - \tfrac{M\tau_n^2}{4}V(Vh_{n-1} + p_{n-1})\right], \ n > 1.$$

Recall Theorem 3.1. If τ_n is sufficiently small then $h_n > h_{n-1}$ must hold.

Furthermore, we may see that

$$\begin{aligned}
&Vh_n + p_n = p_n - p_{n-1} + Vh_{n-1} + p_{n-1} + V(h_n - h_{n-1}) \\
&= p_n - p_{n-1} + Vh_{n-1} + p_{n-1} \\
&+ V\left[\left(I - \tfrac{\tau_n}{2}V\right)^{-1}\left(I + \tfrac{\tau_n}{2}V\right)\left(h_{n-1} + \tfrac{\tau_n}{2}p_{n-1}\right) + \tfrac{\tau_n}{2}p_n - h_{n-1}\right] \\
&= p_n - p_{n-1} + \left(I - \tfrac{\tau_n}{2}V\right)^{-1}\left[\left(I - \tfrac{\tau_n}{2}V\right)(Vh_{n-1} + p_{n-1})\right. \\
&\left. + V\left(I + \tfrac{\tau_n}{2}V\right)\left(h_{n-1} + \tfrac{\tau_n}{2}p_{n-1}\right) + \left(I - \tfrac{\tau_n}{2}V\right)V\left(\tfrac{\tau_n}{2}p_n - h_{n-1}\right)\right] \\
&= p_n - p_{n-1} + \left(I - \tfrac{\tau_n}{2}V\right)^{-1}\left[\left(I - \tfrac{\tau_n}{2}V\right)(Vh_{n-1} + p_{n-1})\right. \\
&\left. + \tau_n V^2 h_{n-1} + \tfrac{\tau_n}{2}V(p_{n-1} + p_n) + \tfrac{\tau_n^2}{4}V^2(p_{n-1} - p_n)\right] \\
&\geq p_n - p_{n-1} + \left(I - \tfrac{\tau_n}{2}V\right)^{-1}\left[\left(I - \tfrac{\tau_n}{2}V\right)(Vh_{n-1} + p_{n-1})\right. \\
&\left. + \tau_n V(Vh_{n-1} + p_{n-1}) + \tfrac{\tau_n^2}{4}V^2(p_{n-1} - p_n)\right] \ = \ p_n - p_{n-1} \\
&+ \left(I - \tfrac{\tau_n}{2}V\right)^{-1}\left[\left(I + \tfrac{\tau_n}{2}V\right)(Vh_{n-1} + p_{n-1}) + \tfrac{\tau_n^2}{4}V^2(p_{n-1} - p_n)\right].
\end{aligned}$$

On the other hand, since $p_n \approx p(h_{n-1} + \tau_n(Vh_{n-1} + p_{n-1}))$ and $p_n > p_{n-1}$, we acquire the following using a Taylor expansion,

$$\begin{aligned}
Vh_n + p_n &\geq p_n - p_{n-1} + \left(I - \tfrac{\tau_n}{2}V\right)^{-1}\left(I - \tfrac{\tau_n}{2}V\right)\left(I + \tau_n V - \tfrac{M\tau_n^3}{4}V^2\right) \\
&\quad \times (Vh_{n-1} + p_{n-1}) \\
&= p_n - p_{n-1} + \left(I + \tau_n V - \tfrac{M\tau_n^3}{4}V^2\right)(Vh_{n-1} + p_{n-1}).
\end{aligned}$$

Similarly, for any sufficiently small τ_n, the matrix $I + \tau_n V - \frac{M\tau_n^3}{4}V^2$ must be positive. Hence the proof is completed. □

Based on Lemmas 4.1 and 4.2, we may state the following theorem for solutions generated by (2.8), (2.9).

Theorem 4.1. *Let (3.3) hold for $0 \leq \ell \leq n$, where $\ell = 0, 1, \cdots, N$, and $h_0 \geq 0$, $Vh_0 + p_0 > 0$. Then the solution sequence $\{h_n\}_{n \geq \ell}$ generated by the semi-adaptive scheme (2.8), (2.9) is strictly monotonically increasing.*

Proof. This result can be viewed as a direct deduction from Lemmas 4.1 and 4.2. □

5. Simulation experiments

Several carefully designed simulation experiments will be presented in the section. Corresponding critical lengths, quenching times, locations will be validated and illustrated for fractional-order reaction-diffusion problem (1.1)-(1.3). Coefficient functions $c(x,t) = b/x$, $d(x,t) \equiv 1$ will be used. The semi-adaptive method (2.8), (2.9) will be employed. The experiments consist of three correlated episodes including the critical lengths, time, and locations of quenches. Numerical results will be carefully compared with existing simulations.

5.1. Critical lengths for quenching

Firstly, we wish to reattain known critical length with $\gamma = 2$, $\psi_0 \equiv 0$ via new semi-adaptive method (2.8), (2.9). To this end, we denote a^* as critical length obtained via the present method, and a^{*M}, a^{*S} as its counterparts obtained via traditional integer order convection-diffusion model equation and analysis in [15,25], respectively. Different values of θ in the source function (1.1) are selected for the purpose of more precise comparisons with known data. The experiments provide a vital initial validation of our scheme.

Table 1 is devoted to selected critical length a^*, as b and θ change. Further, in Fig. 1, we see computed critical lengths a^* when an integer order $\gamma = 2$ is used. It is again found that the value of a^* decreases as θ increases. Fig. 1 provides relative errors of a^*, which is defined as $\left|a^* - a^{*S}\right|/a^*$. The results calculated are consistent with those obtained from the traditional integer order models [15,25].

Table 2 is designed for experiments on correlations between a^*, b and γ. It is found that the critical interval size decreases as b increases from a negative value to zero obviously; while $b > 0$, the relationships between γ and a^* are shown more clearly in Fig. 2 (left frame). It is also valuable to notice the relationship between a^* and γ at a fixed coefficient b. From the right frame of Fig. 2, we may notice that a^* increases monotonically as γ increases for $b < 0.7$ probably; Conversely, when $b \geq 0.7$, a^* decreases monotonically as γ increases.

5.2. Times for quenching

Set the initial temporal step $\tau_1 = (1/2) \times 10^{-4}$ and spatial step $\lambda = a \times 10^{-2}$. Our continuing experimental results are shown in Tables 3, 4, and compared with those obtained by Mooney and Sheng et al. [15,25,26]. Denote T_a^M as the quenching time shown by [25,26], and T_a^S as the quenching time given in [15]. It is clear that our data obtained are well consistent with existing results. Relative errors between T_a and T_a^M and T_a^S are shown precisely in Fig. 3. It is again found that the accuracy of our numerical estimates is highly favorable.

We are particularly interested in the dynamical behavior of T_a as the interval length a tends to the infinity. In our experiments, we observe that the quenching time monotonically decreases in the situation. Some key observation data are shown in Table 5. Apparently the quenching time converges to 0.5 regardless the initial value used. The phenomenon agrees with existing mathematical proofs contained in [15,13]. The monotonicity in convergence is further illustrated through Fig. 4.

The interconnections between T_a and the connection coefficient b are shown in Table 6. Further, in Fig. 5 (left frame), we may see T_a decreases while b increasing when $a = 2$, and $\gamma = 2$ or 1.8 is used. If $b = -0.4$, $\theta = 1.0$ are fixed, then we can show relations between T_a and γ in Table 7. Noticeably, as γ decreases, T_a decays strictly monotonically in most case. Correlation curves between T_a and γ are plotted in Fig. 5. As $a \geq 2$, T_a increases monotonically as γ increases with a range of $\gamma \in \left[(\sqrt{17} - 1)/2,\ 2\right]$.

5.3. Location for quenching

For the purpose of comparisons with existing results, we are particularly interested in cases with $\gamma = 2$, $a = \pi$, $\theta = 1.0$ and $\psi_0 = 0$. Fig. 6 shows not only profiles of the numerical solutions h, h_t immediately prior to quenching, but also trajectories of maximum or supremum of h, h_t, $0 \leq t \leq T_a$, respectively. Simulation method (2.8), (2.9) is again used. Quenching times $T_a \approx 0.5468$ and 0.5304, are detected, respectively. Quenching locations are found approximately at $x^* = 1.6965$ and $x^* = 1.4137$ for cases with $b = -0.4$ and 0.4, respectively. Therefore the solutions h, h_t are not symmetrical. The phenomenon is probably due to the effectiveness of the convective term b/x, however more rigorous proofs in mathematics are still remain open. We may also observe in Fig. 6 that maximum values of the solutions increase strictly monoton-

Table 1
Comparisons between a^* and a^{*M}, a^{*S} over different values of b, θ. $\gamma = 2$ are used.

b	−2.0	−1.2	−0.9	−0.4	0	0.4	0.9	0.95
$a^*, \theta = 1$	2.072582	1.874861	1.794899	1.652212	1.530275	1.414929	1.332568	1.330363
$a^{*M}, \theta = 1$	2.0755	1.8770	1.7968	1.6544	–	1.3935	1.1923	1.1689
$a^{*S}, \theta = 1$	2.0124	1.8280	1.7315	1.6097	–	1.4788	1.4487	1.4479
$a^*, \theta = 2$	1.612341	1.454764	1.391366	1.278776	1.183198	1.093596	1.031212	1.029735
$a^{*S}, \theta = 2$	1.5657	1.4167	1.3576	1.2590	–	1.1283	1.1218	1.1218
$a^*, \theta = 0.5$	2.532675	2.298910	2.203756	2.032898	1.885585	1.744499	1.640060	1.636794
$a^{*S}, \theta = 0.5$	2.5000	2.2389	2.1521	2.0037	–	1.8004	1.7800	1.7800

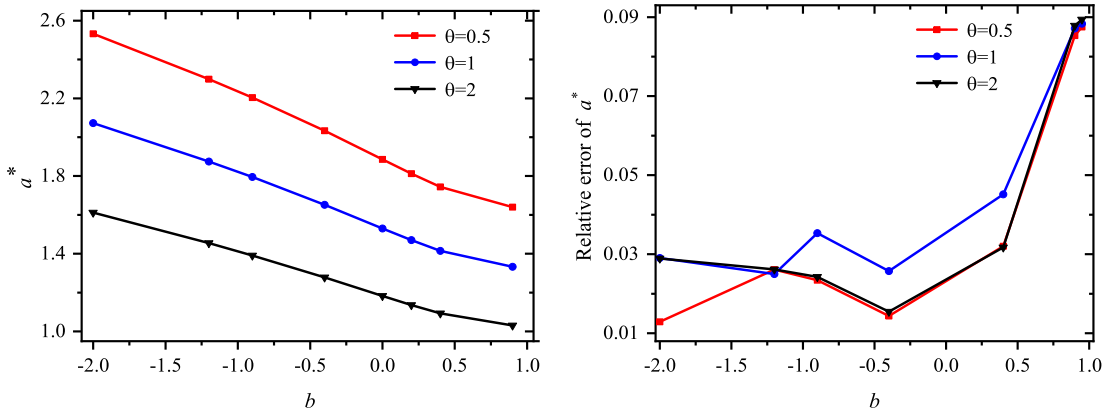

Fig. 1. LEFT: Relations of the critical length a^* *vs.* b and θ. ($\gamma = 2$ is used). RIGHT: Relative error of a^* with a^{*S}. The existing data are from [15,25].

Table 2
To study relations between the fractional order γ, critical length a^* and b, we show the respective values in this table. $\theta = 1$ is employed.

b	−2.0	−1.2	−0.9	−0.4	0	0.4	0.9	0.95
$a^*(b), \gamma = 1.9$	1.962000	1.767995	1.690375	1.552549	1.436666	1.346320	1.336895	1.342391
$a^*(b), \gamma = 1.8$	1.844652	1.654821	1.580026	1.450289	1.343134	1.291261	1.351645	1.362430
$a^*(b), \gamma = 1.7$	1.719696	1.534827	1.462873	1.345548	1.249630	1.248942	1.367042	1.381425
$a^*(b), \gamma = 1.6$	1.586415	1.405574	1.337626	1.230786	1.156019	1.215783	1.379723	1.396771
$a^*(b), \gamma = 1.55$	1.543900	1.343476	1.271266	1.176771	1.109075	1.201368	1.384595	1.402747

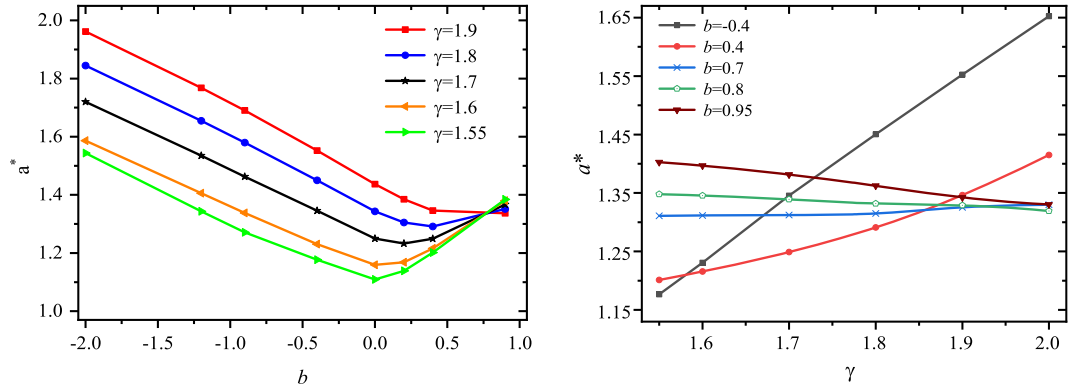

Fig. 2. LEFT: Relations between a^* and b as θ is chosen to be 1, γ is chosen to be $1.9, 1.8, 1.7, 1.6, 1.55$. RIGHT: relations between a^* and γ as $b = -0.4, 0.4, 0.7, 0.8, 0.95$, $\theta = 1$. The figures are based on Table 2. They intend to throw further lights on relationships between the fractional order γ, critical length a^*, and b.

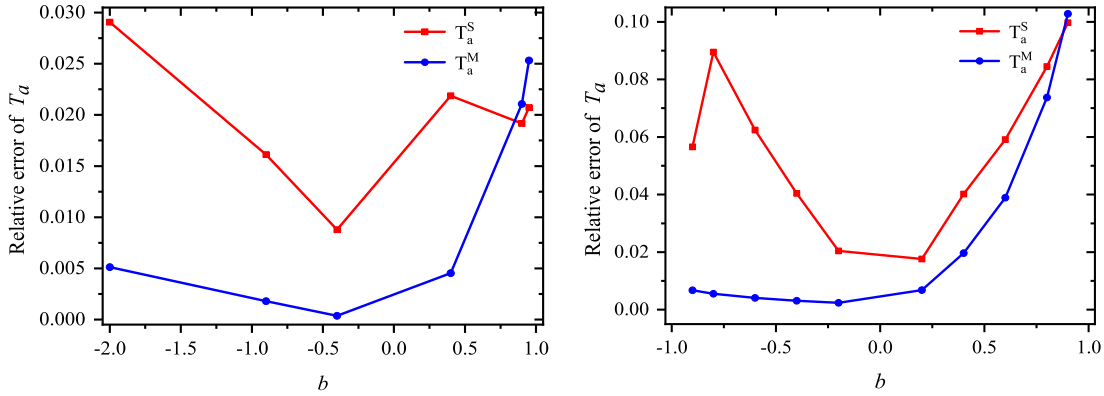

Fig. 3. LEFT: Relative errors between T_a, T_a^S, and T_a, T_a^M, respectively. Values of b are from -2 to 1 with $\gamma = 2$, $a = \pi$, and $\theta = 1$. RIGHT: The same type relative errors when $\gamma = 2$, $a = 2$, and $\theta = 1$ are used. The semi-adaptive scheme (2.8), (2.9) is used.

Table 3
Relations between T_a, T_a^S [15], T_a^M [25,26] and b. Value $\theta = 1$ in (1.1) and the interval length $a = \pi$ are used.

b	−2.0	−0.9	−0.4	0.4	0.9	0.95
T_a	0.5850	0.5580	0.5468	0.5304	0.5220	0.5212
T_a^S	0.568	0.549	0.542	0.542	0.532	0.532
T_a^M	0.588	0.559	0.547	0.528	0.511	0.508

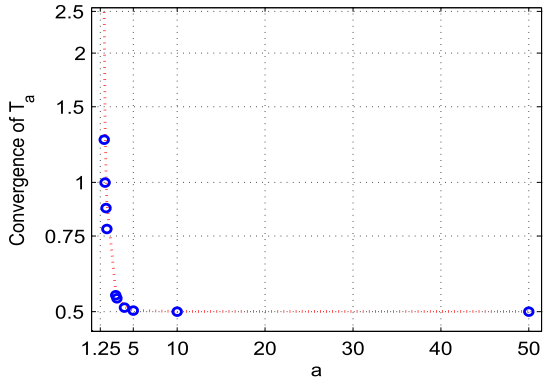

Fig. 4. The monotone convergence of T_a as $a \to \infty$. Circled locations are for data computed earlier in [13,15]. A logarithmic scale is adopted in the y-direction for showing more details.

ically until T_a. Such increments can be dramatical as t approaches to T_a.

A quenching is defined when $\max_{0\le x\le\pi} h(x,T_\pi) \approx 0.9964919$ in our experiments (for $b = 0.4$). We note that for $a = 2$, $b = 0$, $\gamma = 2$ and $\psi(x) = (1/10)\sin(\pi * x/2)$, the integer order quenching model problems offer the value $T_a \approx 0.6964$ [13].

For a more precise description of our numerical solutions, three-dimensional surface plots of h and h_t are given in Fig. 7. The last 20 time levels before quenching are used. Parameters $b = 0.4$, $\theta = 1.0$, $\gamma = 2$ are considered. While $\max_x h$ approaches to the unity at the quenching location $x^* = 1.4137$ steadily, the supremum of the derivative $h_t^* \approx 58.5998446$ exponentially as t is near T_a. The aim to use an integer order $\gamma = 2$ in our first round simulation experiments is to compare our results with existing data stated in [10,15,26,25]. The strong agreement as being seen in Figs. 6, 7 validates remarkably the reliability and effectiveness of the new method (2.8), (2.9).

As for experiments with fractional orders, without loss of generality, we take $\psi_0(x) = 0$ and $a = 2$, $b = -0.4$. We again present profiles of quenching solutions h, h_t in Fig. 8, together with trajectories of the solution and its time derivative. It can be noticed that in Fig. 8, locations of quenching are shifted to the right as γ increases from 1.7 to 1.9.

In fact, the location of quenching is at $x^* \approx 1$ which is the middle point of the spatial interval when $\gamma = 1.8$. When $\gamma < 1.8$, we take $\gamma = 1.7,\ 1.75$ in the experiment, and found that the quenching location shifts leftward from the interval center. For $\gamma > 1.8$, on the other hand, the quenching position shifts from the center point to the right ($\gamma = 1.85,\ 1.9$ are used). This phenomenon can also be seen though Table 8, which gives the maximum, or supremum, values of h, h_t, respectively, and quenching locations.

To further illustrate the solutions computed, we simulate three-dimensional surfaces of h and h_t in Fig. 9. The last 20 time levels immediately before quenching are used. We observe that $\max_{0\le x\le a} h$ approaches to the unity steadily, and $\sup_{0<x<a} h_t^* \approx 47.16637862$ as $t \to T_a \approx 0.7302$ for $\gamma = 1.8$, $\theta = 1$, $b = -0.4$. Our simulations are again consistent with known records in the literature for spatial fractional order quenching problem when $\gamma = 1.8$ [13].

It has been evident in our simulation experiments that the numerical solutions h, h_t do not seem to be symmetric in space for fractional problem such as (1.1)-(1.3). Furthermore, locations of $\max_{0\le x\le a} h(x,t)$ or $\sup_{0<x<a} h_t(x,t)$ do not reappear at the center of the spatial interval considered. This implies that highly reliable and accurate numerical methods are necessary for exploring singular fractional problems such as (1.1)-(1.3).

Fig. 10 shows more profiles of quenching solutions h, h_t immediately before quenching. Semi-adaptive algorithm (2.8)-(2.9) associated with different b values is again utilized. It is visible that as b increases, the quenching location x^* moves to the left. More details of such solutions are given in Table 9.

Finally, recalling truncation errors given by (2.3), (2.4), we may anticipate that the order of convergence for (2.8), (2.9) is approximately linear. However, a rigorous proof of such a conjecture can be challenging due to strong quenching nonlinearity and singularities involved. Fortunately, computational order of convergence estimations via generalized Milne devices have been proved to be extremely effective [23,27]. Adopt the spectral norm. In our experiments, spatial orders of convergences q, r of discrete functions h, h_t are calculated via following formulas, respectively:

$$q_\lambda^\tau(t) = \frac{1}{\ln 2}\ln\frac{\left\|h_\lambda^\tau - h_{\lambda/2}^\tau\right\|_2}{\left\|h_{\lambda/2}^\tau - h_{\lambda/4}^\tau\right\|_2},\quad r_\lambda^\tau(t) = \frac{1}{\ln 2}\ln\frac{\left\|(h_t)_\lambda^\tau - (h_t)_{\lambda/2}^\tau\right\|_2}{\left\|(h_t)_{\lambda/2}^\tau - (h_t)_{\lambda/4}^\tau\right\|_2},$$

where $h_{\lambda/k}^\tau$, $(h_t)_{\lambda/k}^\tau$ are the solution of (2.8), (2.9) and its temporal derivative based on $\tau, \lambda/\ell$, $\ell = 1,2,4$, respectively, and $0 < T_1 \le t \le T_2 < T$. The convergence in time can be evaluated in a similar way, though additional difficulties do occur due to the mesh adaptation, or determined through a Courant number requirement [19]. Now, mark the temporal level of quenching as zero. In Fig. 11, we show computational orders of the convergence of h in final 20 temporal levels, and that

Table 4
A comparison of the relationship between T_a and advection coefficient b, and relationships between T_a^S (given by [15]), T_a^M (given by [25,26]) and b, respectively. $\theta = 1,\ a = 2$ are used.

b	−2.0	−0.9	−0.8	−0.6	−0.4	−0.2	0.2	0.4	0.6	0.8	0.9
T_a	-	1.1522	1.0840	0.9770	0.8962	0.8320	0.7370	0.7018	0.6732	0.6510	0.6420
T_a^S	1.214	1.087	0.987	0.916	0.860	0.815	0.750	0.730	0.713	0.706	0.706
T_a^M	-	1.160	1.090	0.981	0.899	0.834	0.732	0.688	0.647	0.603	0.576

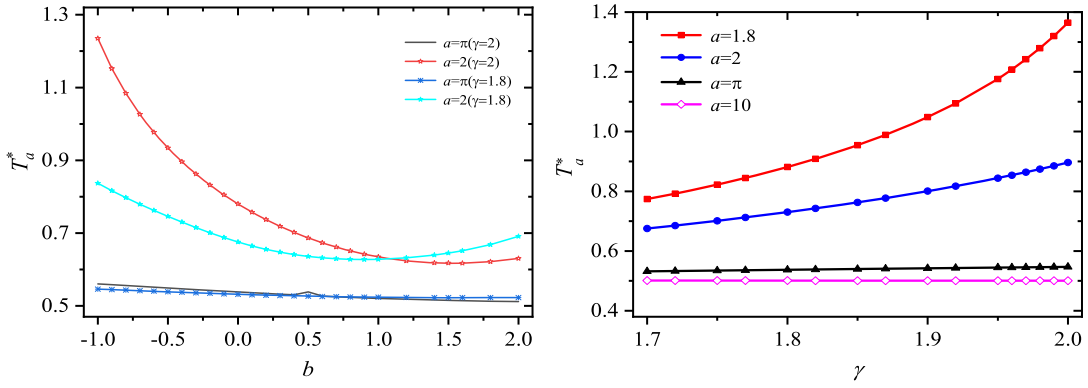

Fig. 5. LEFT: The relation between T_a and the convection coefficient b. RIGHT: The relation between T_a and the fractional order γ. Values of $a = 1.8, 2, \pi$ and 10 are used, respectively.

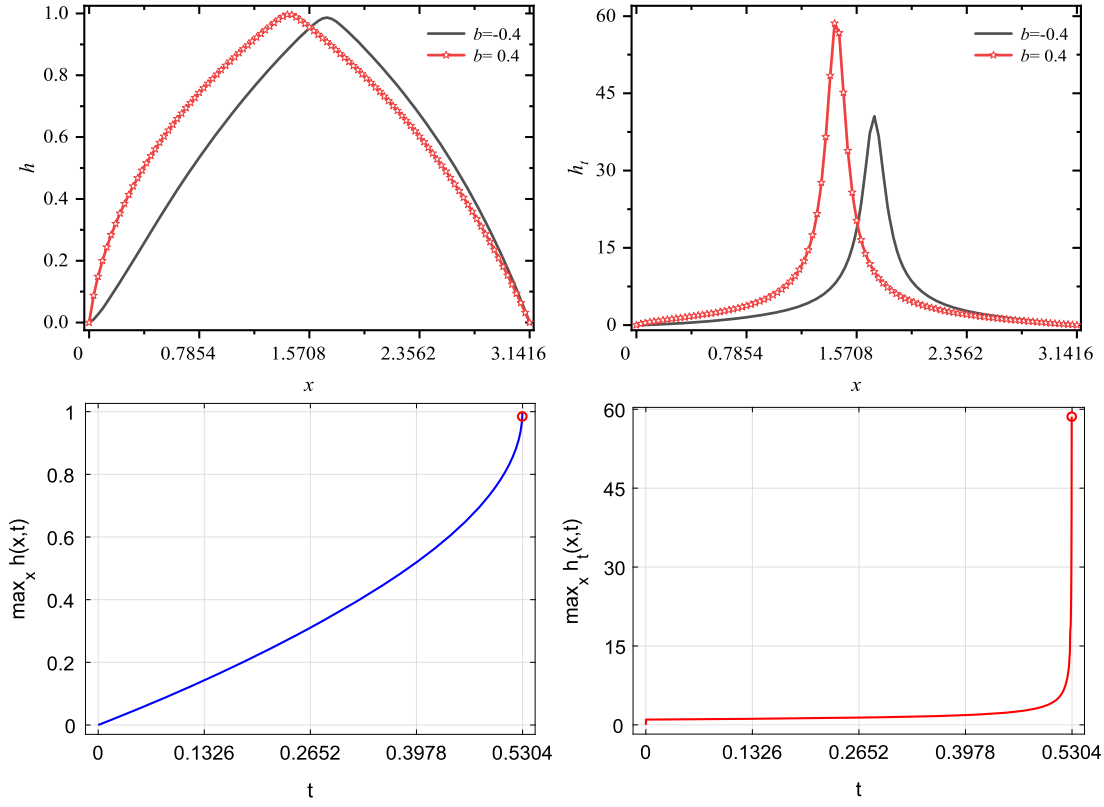

Fig. 6. TOP: Profiles of h and h_t immediately prior to quenching. BOTTOM: Trajectories of $\max_{0\le x\le a} h$ and $\sup_{0<x<a} h_t$ as t increases. The quenching occurs at $T_a \approx 0.5304$ when $\gamma = 2,\ a = \pi,\ b = 0.4,\ \theta = 1.0$.

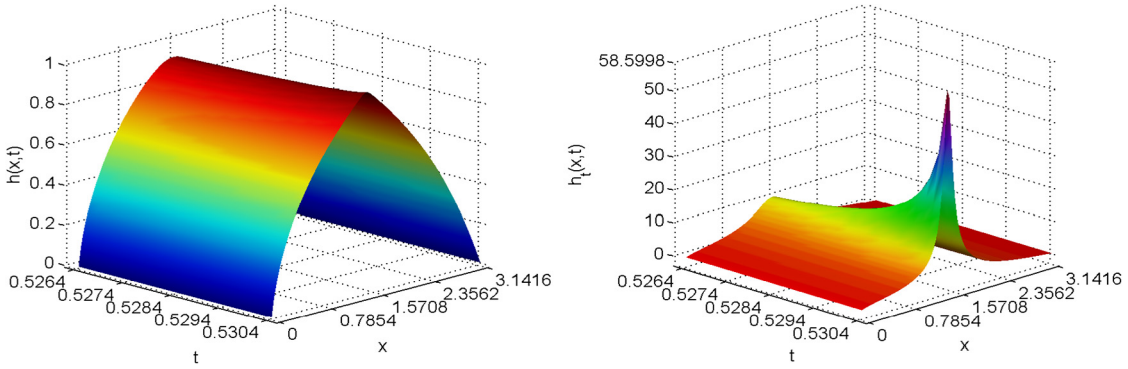

Fig. 7. Three-dimensional surfaces of h and h_t before quenching. Last 20 temporal levels ($0.5264 \le t \le 0.5304$) are used. Parameters $a = \pi,\ \gamma = 2,\ b = 0.4,\ \theta = 1.0$ are employed. The peak value of $h_t(T_a) \approx 58.59984459$.

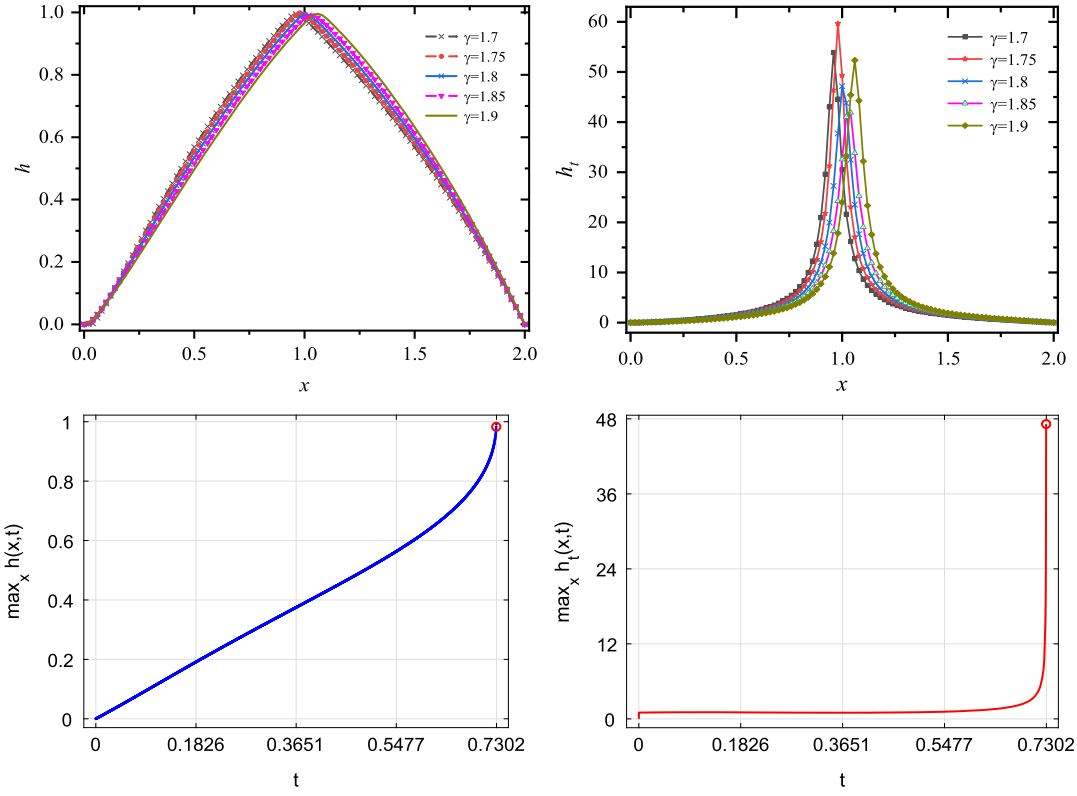

Fig. 8. TOP:Profiles of h and h_t immediately prior to quenching ($\gamma = 1.7, 1.75, 1.8, 1.85, 1.9$ are used). BOTTOM: Trajectories of $\max\limits_{0\le x\le a} h$ and $\sup\limits_{0<x<a} h_t$ as t increases. The quenching occurs at $T_2 \approx 0.7302$ when $b = -0.4,\ \gamma = 1.8,\ a = 2$.

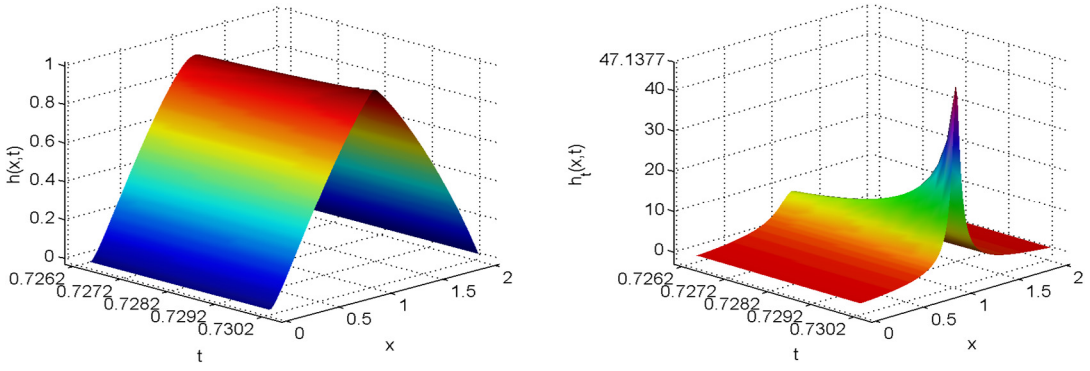

Fig. 9. Three-dimensional surfaces of h and h_t before quenching. Last 20 temporal levels ($0.7262 \le t \le 0.7302$) are used. Parameters $a = 2$ and $\gamma = 1.8$ are employed. The peak value of $h_t(T_a) \approx 47.16637862$.

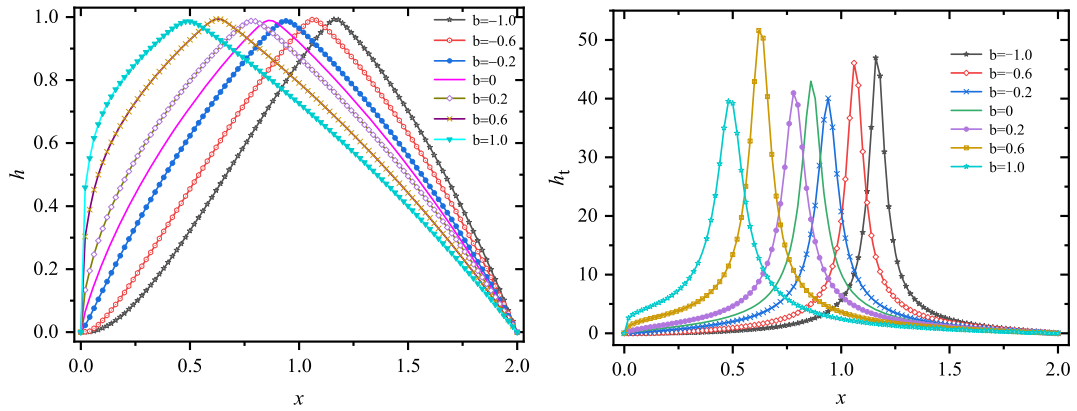

Fig. 10. Quenching location and the advection coefficient b when $a = 2,\ \gamma = 1.8,\ \theta = 1.0$ are used. Simulations results are from the semi-adaptive method (2.8), (2.9).

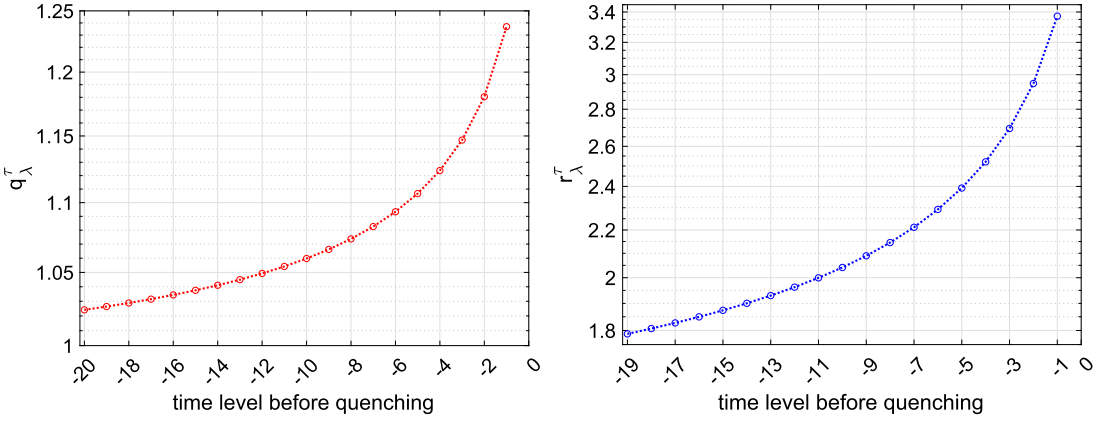

Fig. 11. Computational orders of the convergence of h (LEFT) and h_t (RIGHT). While the mean value of the former is 1.0771, mean value of the latter is 2.1918. The slightly upward trajectories of both estimates may due to the smoothness of the solution h and derivative h_t prior to quenching except in the blow-up area. They may also indicate an acceptable reliability of the finite difference method (2.8), (2.9) as quenching is rapidly approached [15,25,27].

Table 5
The monotone convergence of T_a as $a \to \infty$. $b = -0.4$ and $\theta = 1$ are employed.

a	T_a	a	T_a	a	T_a	a	T_a
1.7	2.4904	2.0	0.8962	4.0	0.5134	10.0	0.5006
1.8	1.3646	3.0	0.5582	5.0	0.5032	30.0	0.5006
1.9	1.0516	π	0.5468	8.0	0.5006	50.0	0.5006

of h_t in final 19 temporal levels immediately before quenching. It is found that the mean value of q_λ^τ is approximately 1.0771 which coincides precisely with our linear convergence expectation. Furthermore, the mean value of r_λ^τ reaches 2.1918 which is slightly elevated, probably due to the strong but relatively localized singularity of h_t shown in Figs. 6–10 in this particular application. Monotonically increasing order trajectories can also be observed in Fig. 11. The phenomenon may imply a satisfactory reliability of the algorithm (2.8), (2.9) in realistic applications as quenching, or fuel combustion, is approached.

6. Conclusions and forthcoming studies

This paper proposes and analyses an accurate numerical method for solving a fractional one-sided quenching type convective-diffusion problem. The constructed method preserves important quenching features. Three key characteristics of the nonlinear quenching model, that is, critical length, time and location for quench, are studied. Computer simulations are provided to illustrate and validate the numerical method accomplished. Numerical solutions obtained are carefully compared with known results [13,15,25]. It is evident that our new scheme is feasible and effective. In particular, our results have revealed the following:

1. Dynamic correlations between the critical length and b. Discussion and simulations are fulfilled for $\gamma = 1.55, 1.6, 1.7, 1.8, 1.9$. When $b < 0$, we find that the critical length decreases monotonically as b increases. On the other hand, when $b = 0.75$, interestingly, the critical length remains the same value $a^* \approx 1.3254$ no matter what fractional order being used within the range.
2. Dynamic correlations between the quenching time T_a and coefficient b. We find the quenching time decreases slightly when b increases. In addition, the value of T_a decreases if a increases. A unique limit of $T_a = 0.5$ is observed as $a \to \infty$. The simulation agrees well with theoretical predictions.
3. All simulation results generated via (2.8)-(2.9) exhibit that the quenching location moves to the right if the fractional order γ increases. The quenching location for the case of $\gamma = 1.8$ is observed at the center point of the spatial interval. For a fixed $\gamma = 1.8$, it seems that the quenching location shifts to left or right whenever b increases or decreases.
4. The mean value of the computational order of convergence is approximately 1.0771 in final 20 temporal advancements before quenching. This can be an indication of a linear convergence of the method (2.8), (2.9) in space. Similar estimates can be made in time. We prefer to leave further simulations to forthcoming papers together with theoretical proofs of the convergence.

Our study reveals more challenges than discoveries in the territory. We have been continuing the endeavor, particularly with multidimen-

Table 6
Relationships among the time of quenching T_a with the coefficient b ($-1.0 \le b \le 2.0, \theta = 1, \psi(x) = 0$).

b	-1.0	-0.6	-0.4	0	0.4	0.6	1.0	1.4	1.8	2.0
T_π, $\gamma = 2$	0.5604	0.5514	0.5468	0.5384	0.5304	0.5268	0.5204	0.5158	0.5126	0.5116
T_2, $\gamma = 2$	1.2352	0.9770	0.8962	0.7800	0.7018	0.6732	0.6346	0.6180	0.6214	0.6304
T_π, $\gamma = 1.8$	0.5460	0.5404	0.5374	0.5316	0.5274	0.5258	0.5238	0.5228	0.5226	0.5226
T_2, $\gamma = 1.8$	0.8370	0.7622	0.7302	0.6754	0.6408	0.6320	0.6278	0.6396	0.6684	0.6912

Table 7
An illustration of the connection between T_a and fractional derivative order γ ($b = -0.4$, $\theta = 1.0$, and $\psi(x) = 0$ are used).

γ	1.65	1.7	1.75	1.80	1.85	1.9	1.95	1.97	2.0
$T_{1.8}$	-	0.7740	0.8222	0.8814	0.9544	1.0484	1.1762	1.2420	1.3646
T_2	-	0.6756	0.7012	0.7302	0.7630	0.8006	0.8442	0.8638	0.8962
T_π	0.5306	0.5322	0.5348	0.5374	0.5400	0.5424	0.5448	0.5456	0.5468
T_{10}	0.5016	0.5014	0.5012	0.5012	0.5010	0.5008	0.5008	0.5006	0.5006

Table 8
Values of $\max_{0\le x\le a} h$ and $\sup_{0<x<a} h_t$ at the quenching locations x^*. Parameters $a = 2$, $b = -0.4$ and $\theta = 1.0$ are used.

γ	1.7	1.75	1.8	1.85	1.9
h^*	0.99519015	0.99812138	0.99242962	0.99013998	0.99609597
h_t^*	53.90493537	59.66890569	47.16637862	41.92559580	52.34520913
x^*	0.96	0.98	1.00	1.04	1.06

Table 9
Peak values of functions $h(x, T_a)$ and $h_t(x, T_a)$ for different b values. Quenching locations are given. Parameters $a = 2$, $\gamma = 1.8$ and $\theta = 1.0$ are used.

b	-1.0	-0.6	-0.2	0	0.2	0.6	1.0
h^*	0.99286124	0.99208711	0.98813508	0.98955723	0.98795306	0.99368668	0.98649343
h_t^*	46.93866893	46.08254310	40.05075059	42.97667669	40.97465890	51.62370180	39.55954883
x^*	1.16	1.06	0.94	0.86	0.78	0.62	0.5

sional fractional partial differential equation models. Numerical studies of effects of fractional convections have been kicked off. Preliminary results suggest that the use of fractional order advection-convection may introduce a much richer dynamics to a combustion environment. These observations need to be further analyzed, evaluated and then verified precisely through laboratory experiments. More details will be given in our forthcoming reports. In addition to continuing endeavors to theoretical proofs of orders of the convergence, more sophisticated and industrially oriented source and degeneracy functions will also be explored [1,8,9,27].

Data availability

The data that has been used is confidential.

Acknowledgements

The authors would like to thank the editor and anonymous reviewers for their time spent and invaluable comments given. Their suggestions have significantly improved the quality and presentation of this paper. The first and second authors are supported in part by the National Science Foundation of China (Grant No. 12062024) and Natural Science Foundation of Ningxia, China (Grant No. 2023AAC03117). The third author is supported partially by the National Science Foundation (Grant No. DMS-2318032) and Simons Foundation (Grant No. MPS-1001466), USA.

References

[1] X.Y. Cao, Z.R. Wang, Y.W. Lu, Y. Wang, Numerical simulation of methane explosion suppression by ultraffne water mist in a conffned space, Tunn. Undergr. Space Technol. 109 (2021) 1–9.
[2] V.A. Kozlovz, M.V. Safonov, Dynamic characteristic of an electrochemical cell with gauze electrodes in convective diffusion conditions, Russ. J. Electrochem. 40 (2004) 460–462.
[3] J. Bollati, A.C. Briozzo, Stefan problems for the diffusion-convection equation with temperature-dependent thermal coefficients, Int. J. Non-Linear Mech. 134 (2021) 103732.
[4] Y. Li, M. Feng, A local projection stabilization virtual element method for convection-diffusion-reaction equation, Appl. Math. Comput. 411 (2021) 126536.
[5] J. Zhang, X.V. Liu, Superconvergence of finite element method for singularly perturbed convection-diffusion equations in 1D, Appl. Math. Lett. 98 (2019) 278–283.
[6] M.M. Meerschaert, C. Tadjeran, Finite difference approximations for fractional advection-dispersion flow equation, J. Comput. Appl. Math. 172 (2004) 65–77.
[7] M.M. Meerschaert, C. Tadjeran, Finite difference approximations for two-sided space-fractional partial differential equations, Appl. Numer. Math. 56 (1) (2006) 80–90.
[8] Q. Sheng, Adaptive decomposition finite difference methods for solving singular problems, Front. Math. China 4 (2009) 599–626.
[9] H. Cheng, P. Lin, Q. Sheng, R. Tan, Solving degenerate reaction-diffusion equations via variable step Peaceman-Rachford splitting, SIAM J. Sci. Comput. 25 (2003) 1273–1292.
[10] H. Kawarada, On solutions of initial-boundary value problems for $u_t = u_{xx} + \frac{1}{1-u}$, Publ. Res. Inst. Math. Sci. 10 (1975) 729–736.
[11] J.K. Hale, Asymptotic Behavior of Dissipative Systems, American Math Soc., Philadelphia, PA, 1988.
[12] A. Acker, W. Walter, The quenching problem for nonlinear parabolic differential equations, Lect. Notes Math. 564 (1976) 1–12.
[13] L. Zhu, Q. Sheng, A note on the adaptive numerical solution of a Riemann-Liouville space-fractional Kawarada problem, J. Comput. Appl. Math. 374 (2020) 466–478.
[14] L. Zhu, N. Liu, Q. Sheng, A simulation expressivity of the quenching phenomenon in a two-sided space-fractional diffusion equation, Appl. Math. Comput. 437 (2023) 127523.

[15] Q. Sheng, A. Khaliq, A compound adaptive approach to degenerate nonlinear quenching problems, Numer. Methods Partial Differ. Equ. 15 (1999) 29–47.
[16] I. Podlubny, Fractional Differential Equations, 1st edition, Academic Press, San Diego, CA, 1998.
[17] L. Zhu, H. Rui, Maximum modulus principle estimates for one dimensional fractional diffusion equation, Appl. Math. J. Chin. Univ. 30 (2015) 466–478.
[18] J.L. Padgett, Solving Degenerate Stochastic Kawarada Partial Differential Equations via Adaptive Splitting Methods, ProQuest LLC, thesis (Ph.D.) Baylor University, Ann Arbor, MI, 2017.
[19] R. LeVeque, Finite Difference Methods for Ordinary and Partial Differential Equations: Steady-State and Time-Dependent Problems, SIAM, Philadelphia, PA, 2007.
[20] Q. Sheng, Y. Ge, A numerical endeavor with nonlinear Kawarada equations, Dyn. Syst. Appl. 25 (2016) 543–556.
[21] M. Beauregard, Numerical approximations to a fractional Kawarada quenching problem, Appl. Math. Comput. 348 (2019) 14–22.
[22] P. Henrici, Discrete Variable Methods in Ordinary Differential Equations, 3rd edition, John Wiley & Sons, New York, NY, 1962.
[23] A. Iserles, A First Course in the Numerical Analysis of Differential Equations, 2nd edition, Cambridge University Press, Cambridge and London, 2009.
[24] Q. Sheng, A. Khaliq, Linearly implicit adaptive schemes for singular reaction-diffusion equations, in: A. Wouwer, P. Saucez, W. Schiesser (Eds.), Adaptive Methods of Lines, CRC Press, London and New York, 2001, pp. 274–305.
[25] J. Mooney, A numerical method for accurate critical length estimation in singular quenching problems, WSSIAA 4 (1995) 505–516.
[26] J. Mooney, An implicit algorithm for iterating to quenching times in degenerate nonlinear parabolic problems, Dyn. Syst. Appl. 5 (1996) 539–551.
[27] J.L. Padgett, Q. Sheng, Numerical solution of degenerate stochastic kawarada equations via a semi-discretized approach, Appl. Math. Comput. 325 (2018) 210–225.